Journal of the European Ceramic Society xxx (xxxx) xxx

Contents lists available at ScienceDirect

Journal of the European Ceramic Society

journal homepage: www.elsevier.com/locate/jeurceramsoc

Evidence for interface-rate limited densification kinetics at Al_2O_3-$GdAlO_3$ interfaces characterized by in situ ultrahigh temperature transmission electron microscopy

D. Keith Coffman [a], Yonghui Ma [b], Christopher Barr [c], Jia-Hu Ouyang [d], Khalid Hattar [c], Shen J. Dillon [a,e,*]

[a] Department of Materials Science and Engineering, University of Illinois at Urbana-Champaign, Urbana, IL 61801, USA
[b] Yantai Research Institute and Graduate School of Harbin Engineering University, Yantai, Shandong 264006, China
[c] Materials, Physical, and Chemical Sciences, Sandia National Laboratories, Albuquerque, NM 87185, USA
[d] School of Materials Science and Engineering, Harbin Institute of Technology, Harbin 150001, China
[e] Department of Materials Science and Engineering, University of California, Irvine, CA 92697, USA

A B S T R A C T

The sintering behavior of single Al_2O_3 particles resting on $GdAlO_3$ is characterized using in situ transmission electron microscopy imaging. In bicrystal experiments, particles with lower Al_2O_3-$GdAlO_3$ phase boundary energies shrink via Ostwald ripening with no evidence of densification that would result from an atomic flux along the interface. Particles with higher Al_2O_3-$GdAlO_3$ phase boundary energies undergo intermittent rigid body motion associated with an interfacial flux mediated by interfacial line defects, e.g. disconnections. Long incubation periods elapse between these comparatively rapid rigid body motion events. The interfacial diffusivity during each event agrees with the magnitude of interfacial diffusion obtained from independent measurements of interfacial diffusivity. The results from the model experiments suggest that capillarity driven interfacial strain mediation, e.g. densification during sintering, is interface rate limited at the driving forces investigated.

1. Background

Understanding the mechanisms of atomic transport along crystalline solid-solid interfaces is critical to engineering high temperature materials and optimizing polycrystalline materials processing. For example, the rapid development of additive manufacturing enables the production of novel sample geometries, but uniform solid-state densification of crystalline materials can be challenging. Although the phenomenology for processes such as grain boundary diffusion, grain growth, creep, sintering, and oxidation are well described [1–5], many features of these processes remain enigmatic in the context of interpreting the effects of intensive variables such as temperature, pressure, chemical potential, or electrical potential [6–8]. For example, the role of common chemical additives in affecting the densification and grain growth of industrially important oxides continues to be debated [9–12]. There has similarly been ongoing controversy about the role of heating rates in affecting sintering rates and the influence of heating methods on microstructural evolution, e.g. Joule heating, microwave heating, optical heating, etc [7,13–18]. When heated rapidly, powder compacts appear to dissipate more interfacial energy via densification than via coarsening as compared to those heated slowly [13,19–21]. This fast–firing effect was originally attributed to the idea that grain growth has a lower activation energy than densification processes, causing the lower temperature evolution of the system to be unfavorable for densification [20]. Indeed, a series of detailed experiments and analyses concluded that low temperature sintering is dominated by non–densifying processes, while densifying processes are more active at high temperatures [19]. This work also demonstrated the effect was relevant to early stages of sintering when grain growth is limited, and coarsening occurs primarily via surface diffusion. Similar effects have been noted in the construction of master sintering curves, wherein the contributions from coarsening at low temperatures may make it difficult to fit the low and high temperature data by a single exponential [22]. Experiments have shown that fast–firing has an additional practical benefit in that the process suppresses residual stress evolution under conditions of constrained sintering [13,23]. A mechanism for this effect remains to be defined. Traditional sintering models such as those developed by Coble [5] and Kuczynski [24] assume diffusion limited kinetics. As a result, the primary temperature dependence for early–stage sintering results from the activation energies for grain boundary diffusion mediated densification and surface diffusion mediated coarsening, when sintering in regimes where lattice and vapor phase transport are negligible. High

* Corresponding author at: Department of Materials Science and Engineering, University of Illinois at Urbana-Champaign, Urbana, IL 61801, USA.
E-mail address: sdillon1@uci.edu (S.J. Dillon).

https://doi.org/10.1016/j.jeurceramsoc.2022.06.001
Received 18 February 2022; Received in revised form 25 May 2022; Accepted 1 June 2022
Available online 3 June 2022

temperature surface diffusivities and grain boundary diffusivities, however, often exhibit activation energies of comparable value. Fig. 1 presents example data from several oxides and metals [25–30]. Under such circumstances, heating rate should not strongly affect the early stages of sintering. The heating rate effect on sintering kinetics, nevertheless, appears to be somewhat general to sintering of a broad variety of materials.

For sintering mediated by vacancy diffusion, densification will result from a flux of vacancies from the surface to grain boundary sinks [31,32]. A sufficient vacancy flux can remove a portion of an atomic plane, an entire atomic plane, or many atomic planes from the grain boundary and deposit those atoms onto a surface. Classical sintering models tend to assume that boundaries are ideal infinite point defect sinks [5], i.e. the process of removing planes of atoms from the boundary occurs continuously because the rate of sink nucleation is not rate limiting. The removal of an atomic plane in a reasonably ordered boundary should occur by the climb of a pre-existing line defect through the interface. Absent such a defect, one must nucleate an interfacial dislocation to serve as a vacancy sink that mediates densification. Relaxing the assumption of the classical sintering models and considering the role of point defect sources and sinks provides an alternative interpretation of the heating rate effect. Ashby [32] hypothesized that sintering could be interface rate limited by the driving force dependence of point defect emission and absorption at sources and sinks. Later authors have developed a grain boundary transport-based model for interface rate limited densification kinetics [33]. However, differences between the predictions of this model and the diffusion limited model are too small to differentiate from isothermal sintering of powder compacts. The processes are expected to exhibit different apparent activation energies, but it has generally been challenging to differentiate such models using activation energy alone [34,35]. It could be argued, in fact, that experimental data has not definitively distinguished reaction rate limited and diffusion limited densification kinetics during sintering despite general acceptance of the diffusion limited model.

Densification following interface rate limited kinetics and coarsening following diffusion limited kinetics could explain the temperature dependence of the sintering trajectory that underpins the efficacy of high heating rate sintering methods. Specifically, it could be anticipated that the activation energy for nucleating grain boundary vacancy sinks exceeds that of grain boundary diffusion. Fig. 2a schematically depicts the temperature dependence of the rates of coarsening and densification under conditions of diffusion-controlled kinetics and interface rate limited kinetics. Fig. 2b schematically depicts the driving force

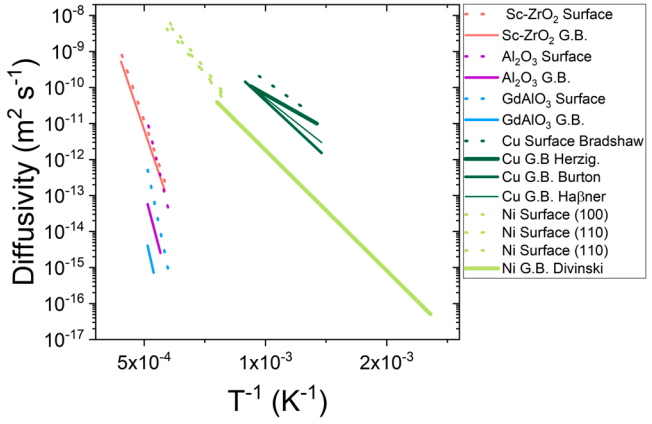

Fig. 1. Activation energies for grain boundary and surface diffusion observed in various oxides and metals [1–4]. Note that the activation energy for grain boundary diffusion is not generally larger than that of surface as would be required to explain the efficacy of fast firing when interpreted in context of diffusion limited models. See notes on other measurements of Ni GB diffusion as a function of purity in Reference [3].

dependence of the densification rate under interface rate limited kinetics at two different temperatures. This schematic figure also highlights how interface rate limited densification kinetics may also help rationalize why high heating rate sintering methods tend to reduce residual stresses during constrained sintering [13,23].

A recent series of experiments performed via in situ bicrystalline Coble creep, zero creep, and sintering in cubic ZrO_2 characterized grain boundary and surface diffusivity, surface energy, grain boundary diffusion mediating point defect formation volumes, the activation volume for creep, and the sintering mechanism [29,30]. Sintering of a particle on a substrate was analyzed in context of Coble's [5] and Kuczynski's [24] classical sintering kinetics models as well as the sintering potential and sintering stress [36]. It was found that surface diffusion mediated coarsening at rates consistent with surface diffusivity. The densification process occurred intermittently, was associated with rotation of the particle, and was found to have an activation barrier. The grain boundary diffusivity calculated from the intermittent densification events agreed well with those measured from the bicrystal Coble creep measurements performed on the same samples. However, between these events no net flux occurred at the grain boundary. It was hypothesized based on both the sintering and creep experiments that the nucleation of grain boundary point defect sources or sinks was kinetically limiting and likely exhibited an energy barrier that could be thermally activated. It was hypothesized that this activation energy barrier associated with vacancy sink nucleation is rate limiting for densification.

A primary concern regarding the hypothesis that sintering of ZrO_2 is generally interface rate limited, however, relates to an inherent problem of studying sintering of small particles on substrates. Gibson and coworkers [37,38] characterized sintering of FCC nanoparticles on substrates, Ag and Cu nanoparticles on Cu, using in situ electron diffraction and plan-view transmission electron microscopy imaging. They observed that only a small fraction of the particles rotated, while the majority exhibited some neck coarsening followed by grain boundary migration through the smaller particle. The same phenomenon was encountered in the ZrO_2 experiments, where the majority of the experiments forming randomly misoriented grain boundaries evolved primarily through grain boundary migration rather than densification and surface diffusion mediated coarsening [29]. The densification, and associated particle rotation, was primarily observed at low-angle grain boundaries and grain boundaries near twin misorientations. As a result, data related to the sintering of so-called random boundaries was not accessible and the hypothesis that densification is interface rate limited is based only on data from so-called special grain boundaries. It is worth noting at this point that during the early stages of sintering of particle compacts geometric constraints likely limit the amount of grain boundary migration that can occur relative to a single particle on a substrate. This problem has been discussed previously within the literature [39]. Regardless, it would be useful to gain insights into whether the densification behavior of arbitrary boundaries tends to follow diffusion limited or reaction rate limited kinetics.

Measurements of interfacial transport, absent grain growth, may be made conveniently in immiscible 2-phase systems [38]. The particle on substrate geometry is convenient to both prepare and analyze. Single interface Coble creep measurements of interfacial diffusion were recently performed in the Al_2O_3-$GdAlO_3$ (GAP) system along with surface diffusivity measurements by capillary smoothing experiments [40]. Those experiments were performed concurrently with the work in this manuscript, allowing for direct comparison under identical experimental conditions. The current work seeks to analyze densification and coarsening during sintering of Al_2O_3-$GdAlO_3$ in particle on substrate geometries where interphase boundary migration is not active. The specific goal of this work is to determine whether transport at these interfaces during sintering follows diffusion limited kinetics or interface rate limited kinetics.

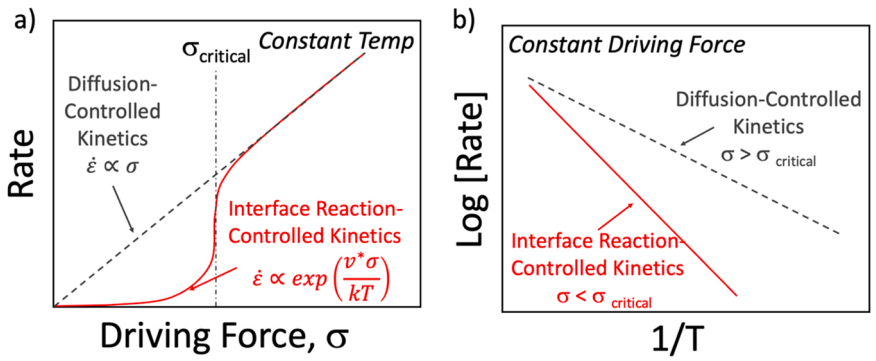

Fig. 2. Schematic comparison of (a) stress and (b) temperature dependence of diffusion limited and interface reaction-rate limited kinetics processes.

2. Experimental

2.1. Procedure

Polycrystalline α-Al_2O_3-$GdAlO_3$ at the eutectic composition, with the addition of 10 vol% SiC, was prepared by hot-pressing at 1500 °C for 1 h at 30 MPa as described in detail elsewhere [41]. A small amount of SiC was added to facilitate IR absorption. The relatively large SiC particles were not observed in the area of interest of this work, but will likely introduce effects associated with silicon and/or carbon doping. These specimens were prepared by mechanical polishing using diamond media and then sputter coated with ≈ 3–5 nm of Au-Pd to suppress charging. This material evaporates in the region of laser irradiation but provides a conductive path to ground. A series of Coble creep experiments were performed, as discussed in a prior manuscript [40], in a highly modified 200 keV JEOL 2100 TEM equipped with a 20 W 1064 nm laser aligned colinearly with the electron beam and focused to an approximately 50 μm spot. A schematic of the testing Geometry is shown in Fig. S1. Such creep experiments may be used to generate high curvature asperities and geometries away from local equilibrium. The relaxation of geometries away from local equilibrium, which also contain an interface, are the basis for the in situ sintering behavior analyzed here. Image sequences are obtained at an average frame rate of ≈ 6 frames per second. The benefit of the approach is that it does not require focused ion beam milling, it can be used to generate randomly oriented interfaces, and measurements of diffusion have already been made under identical experimental conditions. Since the in situ sintering behavior characterized here occurs just after in situ Creep experiments, the entire process is observed without thermal cycling. Initial times cited for the analysis, thus, represent a first isothermal observation. The prior paper provides additional details related to temperature calibration [40], which was performed using electron diffraction measurements of lattice parameter expansion where the data were referenced to the melting temperature. For comparison, one Al_2O_3-$GdAlO_3$ eutectic sample, prepared following details found elsewhere [42], was prepared in pillar geometries using focused ion beam milling (FIB, FEI Helios). Prior work suggests that the threshold for knock-on electron beam damage in Al_2O_3 is ≈ 300 keV, but electrostatic charging could influence the damage process, particularly at temperatures where ions are mobile. Experiments were performed at beam current densities on the order of 1 mA cm^{-2}. No apparent electron beam induced reactions or kinetics were observed in this system during imaging at fluxes of ≈ 100 mA cm^{-2}. Prior in situ measurements of surface and grain boundary diffusion under the same imaging conditions obtained values reasonably consistent with those previously reported in the literature. This is consistent with our expectation of limited electron beam influence on the process.

Model 2-particle sintering geometries were analyzed, where one particle was observed to be resting on the sample after the tensile creep experiment concluded: these experiments were discussed in Ref. [40]. The results are analyzed in the context of the sintering potential, Σ, defined as the change in free energy per unit length of densification, associated with a reduction in surface energy and curvature. This quantity was first conceptualized in zero creep experiments, by Udin et al [43]., used to measure surface energies and takes the general form;

$$\Sigma = \pi r \gamma_s \Lambda \tag{1}$$

where r is the radius of the interface, γ_s is the surface energy, and Λ is a unitless function of the particle geometry and interfacial energies. A generalized model was derived by Cannon and Carter [36], which accounts for surface curvature and triple junction geometry;

$$\Sigma = \pi r \gamma_S (2\cos\varphi - \kappa r) \tag{2}$$

where κ is the curvature and φ is the turning angle at the triple junction, which is the angle between the tangent to the surface and the grain boundary plane. Our particles were not necessarily spherical, due either to anisotropic surface energy or the kinetic evolution. In this case the mean curvature was taken as the sum of the radial curvature (assuming a surface of revolution) and a mean projected curvature defined by the convex hull and turning angles, following the von-Neumann-Mullins formula.

$$\kappa = \frac{cos\phi}{r} + \frac{2\pi - \phi_1 - \phi_2}{\varsigma} \tag{3}$$

where ς is the convex hull perimeter. To avoid uncertainty associated with the surface energy values used, the results are discussed in the context of a reduced sintering potential, defined as Σ/γ_S. Similarly, a reduced sintering stress, σ_s/γ_S is calculated as the reduced sintering potential divided by the grain boundary neck area, $A = \pi r^2$, which is assumed to be approximately circular. The reader should be aware that the assumptions about 2-D versus 3-D geometry could introduce errors in the analysis. This is likely the largest potential source of error. It may be reasonable to expect the circular neck assumption may be produce an error that is at most a factor of 5, since GB error would vary linearly with the under/overestimation of neck thickness. Such an error does not fundamentally affect any of the conclusions in the manuscript but might affect the magnitudes of the reported sintering stresses. Measurement of the dihedral angles is also sensitive to alignment of the interfacial plane with the electron beam. The calculated value of Σ, however, is only weakly dependent on the dihedral angle since the dihedral angle related terms in Eqs. (2) and (3) mostly cancel one another. This error is, therefore, anticipated to be small relative to the aforementioned error.

Under diffusion-limited transport along the boundary, the normal interfacial stress distribution is defined by neck surface boundary conditions of interface radius and curvature, derived by Johnson [44], as well as Cannon & Carter [36].

$$\sigma(\tilde{r}) = C_1\left(1 - \frac{\tilde{r}^2}{r^2}\right) - \kappa\gamma_s \tag{4}$$

$$C_1 = \kappa\gamma_s - \frac{2\pi r\gamma_s cos\phi}{\pi r^2} + \frac{F_a}{\pi r^2} \quad (5)$$

where $\tilde{r}$ is the radial coordinate along the interface and F_a is an applied force, which is zero for the case of unconstrained particles on a substrate. This can also be written as

$$\sigma(\tilde{r}) = \frac{2}{\pi r^2}(F_a - \Sigma)\left(1 - \frac{\tilde{r}^2}{r^2}\right) - \kappa\gamma_s \quad (6)$$

The rate of sintering dL/dt due to interfacial diffusion under this condition is

$$\frac{dL}{dt} = \frac{\Omega\delta D_i}{kT}\nabla^2\sigma = -\frac{\Omega\delta D_i}{kT}\frac{8}{\pi r^4}(F_a - \Sigma) \quad (7)$$

Where D_i is the interfacial diffusivity, δ is the diffusion boundary thickness, Ω is the atomic volume, and kT is the thermal energy. This equation can be inverted to measure interfacial diffusivity from the geometric evolution of the particle, if the material parameters are known.

$$D_i = \frac{dL}{dt}\frac{kT}{8\Omega\delta}\frac{\pi r^4}{(F_a - \Sigma)} \quad (8)$$

Image analyses were performed using custom Matlab scripts.

3. Results

Two general types of behavior were primarily observed regarding the structural evolution of Al_2O_3 particles resting on $GdAlO_3$. Examples of each are shown in Figs. 3 and 4 and Videos 1 and 2 for experiments performed at T ≈ 1674 °C and T ≈ 1628 °C, respectively. In the first case, Fig. 3, the Al_2O_3 shrinks continuously with approximately constant dihedral angles; presumably primarily via Ostwald ripening by surface diffusion to neighboring Al_2O_3 grains. The relatively large dihedral angles, 130–135°, suggest that this Al_2O_3-GAP interface is relatively low energy. No apparent rotation of the particle is observed. The center of mass of the particle can move via both the Ostwald ripening and densification in this unconstrained geometry. The process is continuous, with no discrete displacement of the particle on short timescales. Based on prior measurements of interface diffusion under the same experimental conditions, the time necessary to remove a plane of atoms from the boundary under diffusion limited kinetics in this example should be on the order of 0.1 s. No interface transport mediated processes are apparent in this data. In other examples, such as shown in supplementary Fig. S1, $GdAlO_3$ nanoparticles resting on the Al_2O_3 particle surface serve as reference markers and clearly demonstrate no observable rigid body motion resulting from interfacial diffusion. It is, thus, concluded that the interfacial diffusion contribution to the evolution of this particle is negligible. At the highest temperatures some vapor phase transport may also be active, since Al_2O_3 loss from the surface was observed above T ≈ 1628 °C. For example, the equilibrium vapor pressure of Al_2O_3 at 1600–1700 °C has been cited to be on the order of 10^{-4} to 1 torr [45], but the evaporation rate is highly sensitive to H_2/H_2O ratio. The evaporation rate depends on interface kinetics and is challenging to calculate explicitly. The rate, however, is anticipated to be low on the timescale of the observation. For example, prior experiments demonstrated the growth of Al_2O_3 nanowires under steady-state bicrystal creep over similar timescales [40]. Those nanowire structures were geometrically stable against evaporation during growth. The coarsening process, furthermore, does not affect the prevalence of interfacial diffusion or the thermodynamic analysis discussed below. Fig. 3 plots the reduced sintering stress as a function of time. The sintering stress decreases slowly as the Al_2O_3 particle shrinks via Ostwald ripening. The value is on the order of 10^6 m^{-1}, throughout the experiment. If, for example, the surface energy is ≈ 1 J m^{-2} then the stress would be on the order of 10^6 Pa.

Supplementary material related to this article can be found online at

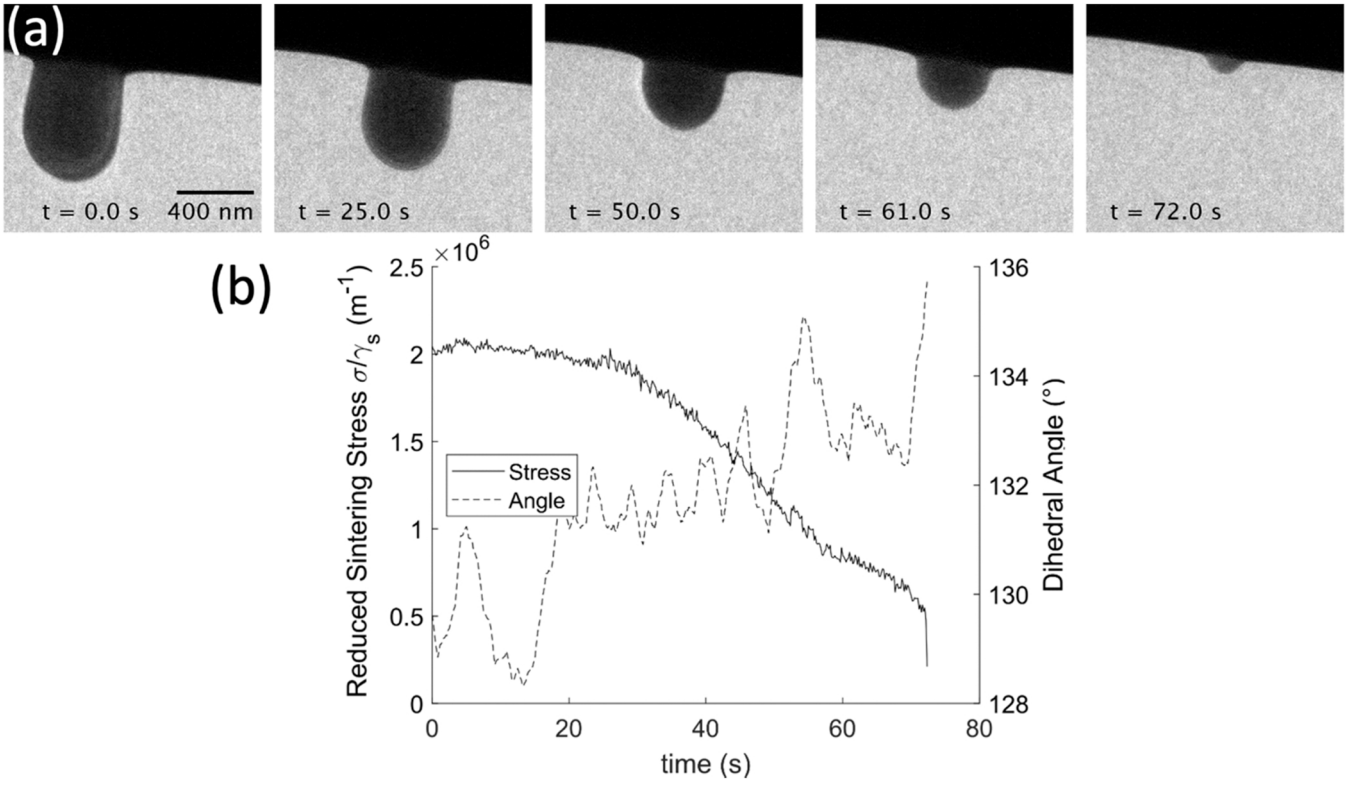

Fig. 3. (top) Capillary evolution of Al_2O_3 asperity in a continuous mode. (bottom) plot of the reduced sintering stress and dihedral angle as a function of time. The dihedral angle in this case varies weakly in time and the sintering stress gradually decreases. Note that t = 0 represents the beginning of the video sequence analyzed as opposed to the structure prior to heating.

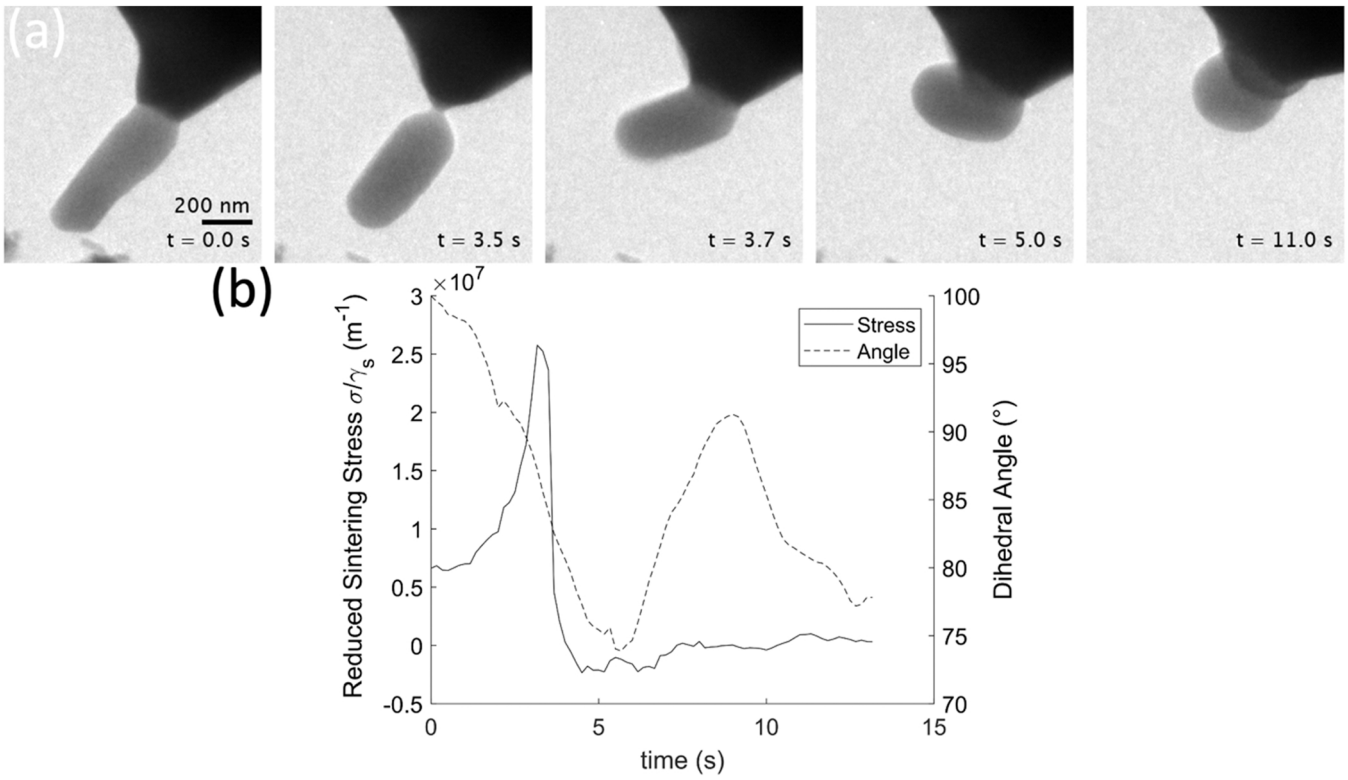

Fig. 4. (top) Capillary evolution of Al_2O_3 asperity at T ≈ 1628 °C. (bottom) plot of reduced sintering stress and dihedral angle as a function of time. As the particle shrinks via Ostwald ripening the neck begins to shrink faster, increasing the sintering stress. The dihedral angles decrease at the same time, suggesting that the interfacial energy is increasing. At a critical stress the particle undergoes rapid rigid body motion, including rotation, this reduces the sintering stress and is effectively a densification process. In this case, after rotation the interphase boundary is not parallel to the electron beam and the measurements of dihedral angle cannot be accurate. It is anticipated that the dihedral angles should increase again as observed in several of the examples shown in the supplementary data.

doi:10.1016/j.jeurceramsoc.2022.06.001.

In the second case, as shown in Fig. 4, the Al_2O_3 grain initially shrinks continuously via Ostwald ripening. Transient increases in sintering stress, however, occur just prior to rapid rotation of the Al_2O_3 particle. The rotation angles observed for this type of behavior were as large as ≈ 90° in some cases. The rigid body rotation is taken as evidence for an interface process mediated by a defect with a Burger's vector. The rigid motion of the Al_2O_3 particle's center of mass toward the GAP is indicative of densification. The rotation and densification suggest that the process is mediated by a combination of interfacial dislocation glide and climb. At this temperature, the interfacial diffusivity is sufficiently facile that these events may appear to be discrete on the time scale of the imaging rate. Based on Eq. (8) a plane of atoms could be removed from the interface via the climb of an interface dislocation at timescales on the order of 10^{-3}–10^{-1} s depending on the interface width at the point of observation. At an imaging rate of 6 frames per second, these events are, thus, anticipated to give the appearance of a discrete process, as is observed experimentally. Fig. 4b plots the measured reduced sintering stress along with the dihedral angles. On average the relative sintering stress for the data in Fig. 4b is larger than in Fig. 3b. A maximum sintering stress is reached just prior to rotation and is on the order of 10^7 m^{-1}. The dihedral angles for this particle are smaller than those observed in Fig. 3, in this case ≈ 75–100°. This dihedral angle decreases just prior to rotation of the particle, which indicates that the interfacial energy also increases prior to the event. The total free energy of the system cannot spontaneously increase, and it is hypothesized that the interfacial free energy increase is driven by dissipation of surface energy through the Ostwald ripening process. The increase in interfacial free energy can drive it over an energy barrier associated with accessing metastable states, such as the nucleation of an interfacial dislocation.

Several examples of particles evolving in a manner like those in Figs. 3 and 4 are plotted in the supplementary data, Figs. S2–6. All observations fall into one of these two distinct types of behavior, where relatively high energy interfaces undergo transient rigid body motion associated with overcoming an activation barrier and relatively low energy barriers shrink via Ostwald ripening with no apparent rigid body motion. Since the sub-surface topology is not easily visible in the TEM images, it is reasonable to ask whether particles like those in Fig. 3 shrink via surface diffusion or relax into a neighboring pore. To verify that Ostwald ripening indeed drives such particle shrinkage, a pillar geometry was prepared by focused ion beam milling across a relatively low-energy Al_2O_3-$GdAlO_3$ eutectic interface. This enables the supporting materials to be clearly visible. As shown in Fig. S7, the Al_2O_3 particle shrinks via Ostwald ripening and exhibits no rigid body motion.

4. Discussion

Observations of model 2-particle sintering herein, where one particle is constrained and the other is unconstrained, generally agree with the hypothesis that the densification rate is not diffusion limited for particles of radius ≈ 100 nm – 1 μm, i.e. the range measured here. At lower energy interfaces, Ostwald ripening occurred with essentially no densification or rigid rotation. This suggests that surface diffusion is much more facile even though Al_2O_3 surface diffusivity and Al_2O_3-GAP interfacial diffusivity are of similar magnitude at the temperatures investigated [40]. Thus, the rate limiting kinetic mechanism at the interface cannot be diffusion under the experimental conditions investigated here. At relatively high energy interfaces, where grain boundary transport was intermittently active, with long incubation times lapsing between events. During each rigid body motion event, the kinetics were reasonably consistent with the interfacial diffusivity within the constraints of the geometric assumptions and the temporal resolution of our

observations. The large rotation angles observed are hypothesized to reduce the interfacial energy after rotation. This is observed in several cases where the interface plane after rotation is still well aligned with the direction of observation in the TEM. This hypothesis is supported by an observation of higher dihedral angles and a higher relative sintering potential after the rotation event, suggesting the formation of a lower energy interface. The results suggest that nucleation of such defects occurs more readily at high energy interfaces relative to low energy interfaces where no such nucleation was observed. The transient increase in interfacial energy, must occur with an overall decrease in the total Gibbs free energy of the system. Since the only driving force for reduction in the overall free energy is coarsening, this process likely provides the driving force for the local increase in the free energy of the Al_2O_3-GAP interface.

Densification following interface rate limited kinetics will have important implications on stress evolution during sintering. Stresses evolved in a diffusion limited densification model can relax continuously. Systems that evolve following interface rate kinetics may intermittently stabilize stresses up to a critical stress associated with nucleating a strain mediating interfacial vacancy sink. The mechanism should also influence expectations related to the role of temperature and heating rate in affecting the sintering trajectory. The magnitude of the activation barrier for point defect sink nucleation could influence the relative rates of Ostwald ripening and densification during the early stages of sintering at different temperatures.

The experimental observations here are qualitatively similar to recent molecular dynamics simulations of the sintering of 20 nm Ni particles of grain boundaries of different crystallographic character [46]. The work equilibrated bicrystal geometries, calculated the associated grain boundary diffusivities and energies, and then removed bounding atoms from the cell to create particles from those pre-equilibrated interfaces. The high energy interfaces underwent densification and particle rotation and the highest rate of densification [46]. The lowest energy boundaries did not exhibit measurable densification, i.e. on the order of 1 at. plane. All the boundaries underwent densification at rates considerably slower than predicted by inputting the calculated diffusivities into the classical sintering models. The discrepancy was similarly attributed to the mixed mechanisms being active, e.g. diffusion and defect sink nucleation. Although each particle rotated suggesting interfacial line defect motion, two thirds of the particles exhibit densification strain of magnitude less than a lattice Burger's vector suggesting little densification, wherein apparent strain could also result from surface diffusion in the 2 particle configuration [46]. The driving force associated with nanoparticle sintering is considerably higher than the experiments herein, and the simulation timescales are considerably slower. The effects of anisotropy observed in the simulations, nevertheless, follow the same trend as the current experiments. Namely, high energy interfaces tend to have lower barriers to the nucleation of densification mediating interfacial line defects and that the average densification kinetics are considerably slower than anticipated from interfacial diffusivity alone due to the kinetic being rate limited by line defect nucleation.

It is noted that it may be too early to generalize these results too broadly to a range of systems of different particle sizes and chemistry, or to later stages of sintering that may exhibit more complex stress states and more facile grain growth. The recent experimental and computational results, however, suggest that accounting for interface rate limited kinetics within the context of sintering could have important implications both on interpreting the literature and engineering the sintering process. For example, the results suggest that it may not generally be prudent to use densification rates as the basis for calculating grain boundary diffusivity without independent confirmation of the rate limiting mechanism [5,44]. The effects of sintering additives have commonly been interpreted in the context of their influence on interfacial diffusivities. In context of interface rate limited kinetics, additive effects could also be interpreted in context of their influence on the thermodynamics of interfacial line defect nucleation. The results could also help explain why shear stresses may enhance densification [47,48], possibly via the role of shear in promoting vacancy sink line defect nucleation. The magnitude of the activation energy for the interface rate limited process might also influence the overall sinterability of differ types of crystalline materials. Of current technological interest is the uniform densification of complex structures prepared by additive manufacturing, especially in context of composite structures sensitive to differential sintering. The critical stress barrier associated with interface rate limited kinetics will define the stress below which stress relaxation is inefficient. This stress and temperature is, thus, expected to strongly influence residual stress evolution and the uniformity of densification. Measuring this temperature dependence will be the subject of future work.

5. Conclusions

This work primarily demonstrated that randomly oriented Al_2O_3 particles on $GdAlO_3$ evolve either essentially purely through Ostwald ripening with no apparent contribution from a flux at the solid interface, or via intermittent rigid body motion that has an associated activation barrier. The results indicate that, in the regime of driving force studied, average transport at the interphase boundary follow reaction rate limited kinetics. The difference in the two types of response is attributed to lower energy interfaces exhibiting higher interfacial line defect nucleation activation energies that limits their ability to activate at the driving forces and temperatures measured. Higher energy interfaces appear to, on average, exhibit lower activation energies making their average densification kinetics more facile.

Declaration of Competing Interest

The authors declare that they have no known competing financial interests or personal relationships that could have appeared to influence the work reported in this paper.

Acknowledgments

Support from US National Science Foundation under Grant DMR 1922867 is acknowledged by K.C and S.J.D. C.M.B. and K.H. were supported by the US Department of Energy, Basic Energy Sciences, Materials Science and Engineering Division under FWP 15013170. This work was performed, in part, at the Center for Integrated Nanotechnologies, an Office of Science User Facility operated for the U.S. Department of Energy (DOE) Office of Science. Sandia National Laboratories is a multimission laboratory managed and operated by National Technology and Engineering Solutions of Sandia, LLC, a wholly owned subsidiary of Honeywell International, Inc., for the U.S. DOE's National Nuclear Security Administration under contract DE-NA-0003525. The views expressed in the article do not necessarily represent the views of the U.S. DOE or the United States Government. Y.H.M and Jh.O. acknowledge Natural Science Foundation of China for the supports in this work under Grant Nos. 51972085, 51572061 and 51621091.

Appendix A. Supporting information

Supplementary data associated with this article can be found in the online version at doi:10.1016/j.jeurceramsoc.2022.06.001.

References

[1] J.E. Burke, D. Turnbull, Recrystallization and grain growth, in: Progr. in Metal Phys, 3, Interscience Publishers Inc, 1952, pp. 220–292.
[2] M. Hillert, The theory of normal and abnormal grain growth, Acta Metall. 13 (3) (1965) 227–238.
[3] N. Cabrera, N.F. Mott, Theory of oxidation of metals, Rep. Prog. Phys. 12 (1949) 163–184.

[4] C. Wagner, Reaction types in the oxidation of alloys, Z. Elektrochem. Angew. Phys. Chem. 63 (1959) 772–782, discussion 782-90.
[5] R.L. Coble, Initial sintering of alumina and hematite, J. Am. Ceram. Soc. 41 (1958) 55–62.
[6] H. Conrad, D. Yang, Influence of an applied dc electric field on the plastic deformation kinetics of oxide ceramics, Philos. Mag. 90 (9) (2010) 1141–1157.
[7] M. Cologna, B. Rashkova, R. Raj, Flash sintering of nanograin zirconia in <5 s at 850°C, J. Am. Ceram. Soc 93 (11) (2010) 3556–3559.
[8] P.R. Cantwell, et al., Grain boundary complexions, Acta Mater. 62 (2014) 1–48.
[9] S.-J.L. Kang, What we should consider for full densification when sintering, Materials 13 (16) (2020).
[10] R.K. Bordia, S.-J.L. Kang, E.A. Olevsky, Current understanding and future research directions at the onset of the next century of sintering science and technology, J. Am. Ceram. Soc. 100 (6) (2017) 2314–2352.
[11] M. Biesuz, V.M. Sglavo, Flash sintering of ceramics, J. Eur. Ceram. Soc. 39 (2–3) (2019) 115–143.
[12] Y. Dai, et al., The physical chemistry and materials science behind sinter-resistant catalysts, Chem. Soc. Rev. 47 (12) (2018) 4314–4331.
[13] C. Wang, et al., A general method to synthesize and sinter bulk ceramics in seconds, Science 368 (6490) (2020) 521.
[14] J. Croquesel, et al., Direct microwave sintering of pure alumina in a single mode cavity: grain size and phase transformation effects, Acta Mater. 116 (2016) 53–62.
[15] R. Raj, M. Cologna, J.S.C. Francis, Influence of externally imposed and internally generated electrical fields on grain growth, diffusional creep, sintering and related phenomena in ceramics, J. Am. Ceram. Soc 94 (7) (2011) 1941–1965.
[16] Z.A. Munir, U. Anselmi-Tamburini, M. Ohyanagi, The effect of electric field and pressure on the synthesis and consolidation of materials: a review of the spark plasma sintering method, J. Mater. Sci. 41 (3) (2006) 763–777.
[17] Z. Shen, et al., Spark plasma sintering of alumina, J. Am. Ceram. Soc. 85 (8) (2002) 1921–1927.
[18] R. Roy, et al., Full sintering of powdered-metal bodies in a microwave field, Nature 399 (6737) (1999) 668–670.
[19] M.-Y. Chu, et al., Effect of heating rate on sintering and coarsening, J. Am. Ceram. Soc. 74 (6) (1991) 1217–1225.
[20] M.P. Harmer, R.J. Brook, Fast firing - microstructural benefits, Trans. J. Br. Ceram. Soc. 80 (5) (1981) 147–149.
[21] W. Ji, et al., Ultra-fast firing: effect of heating rate on sintering of 3YSZ, with and without an electric field, J. Eur. Ceram. Soc. 37 (6) (2017) 2547–2551.
[22] H. Su, D.L. Johnson, Master sintering curve: a practical approach to sintering, J. Am. Ceram. Soc 79 (12) (1996) 3211–3217.
[23] J.S.C. Francis, et al., Flash sintering of anode-electrolyte multilayers for SOFC applications, J. Am. Ceram. Soc. 96 (5) (2013) 1352–1354.
[24] G.C. Kuczynski, Self-diffusion in sintering of metallic particles, Trans. Am. Inst. Min. Metall. Pet. Eng. 1 (2) (1949) 169–178 (Trans).
[25] P.S. Maiya, J.M. Blakely, Surface self-diffusion and surface energy of nickel, J. Appl. Phys. 38 (2) (1967) 698–704.
[26] S.V. Divinski, G. Reglitz, G. Wilde, Grain boundary self-diffusion in polycrystalline nickel of different purity levels, Acta Mater. 58 (2) (2010) 386–395.
[27] F.J. Bradshaw, R.H. Brandon, C. Wheeler, The surface self-diffusion of copper as affected by environment, Acta Metall. 12 (9) (1964) 1057–1063.
[28] T. Surholt, C. Herzig, Grain boundary self-diffusion in Cu polycrystals of different purity, Acta Mater. 45 (9) (1997) 3817–3823.
[29] R.L. Grosso, et al., Ultrahigh temperature in situ transmission electron microscopy based bicrystal coble creep in Zirconia II: Interfacial thermodynamics and transport mechanisms, Acta Mater. 200 (2020) 1008–1021.
[30] K.S.N. Vikrant, et al., Ultrahigh temperature in situ transmission electron microscopy based bicrystal coble creep in zirconia I: nanowire growth and interfacial diffusivity, Acta Mater. 199 (2020) 530–541.
[31] J. Han, S.L. Thomas, D.J. Srolovitz, Grain-boundary kinetics: a unified approach, Prog. Mater. Sci. 98 (2018) 386–476.
[32] M.F. Ashby, On interface-reaction control of Nabarro-Herring creep and sintering, Scr. Metall. 3 (11) (1969) 837–842.
[33] A.C.F. Cocks, Overview no. 117 The structure of constitutive laws for the sintering of fine grained materials, Acta Metall. Mater. 42 (7) (1994) 2191–2210.
[34] Z. He, J. Ma, Constitutive modelling of the densification of micron-grain-sized alumina ceramics, Philos. Mag. 83 (16) (2003) 1889–1916.
[35] Z. He, J. Ma, Constitutive modeling of alumina sintering: grain-size effect on dominant densification mechanism, Comput. Mater. Sci. 32 (2) (2005) 196–202.
[36] R.M. Cannon, W.C. Carter, Interplay of sintering microstructures, driving forces, and mass transport mechanisms, J. Am. Ceram. Soc. 72 (8) (1989) 1550–1555.
[37] M. Yeadon, et al., In-situ observations of classical grain growth mechanisms during sintering of copper nanoparticles on (001) copper, Appl. Phys. Lett. 71 (12) (1997) 1631–1633.
[38] M. Yeadon, et al., Sintering of silver and copper nanoparticles on (001) copper observed by in-situ ultrahigh vacuum transmission electron microscopy, Nanostruct. Mater. 10 (5) (1998) 731–739.
[39] F.F. Lange, Densification of powder compacts: an unfinished story, J. Eur. Ceram. Soc. 28 (7) (2008) 1509–1516.
[40] K. Coffman, et al., Interphase Boundary, Grain Boundary, and Surface Diffusion in Al2O3-GdAlO3 Composites Determined from Bicrystal Coble Creep Experiments, J. Eur. Ceram. Soc. 42 (9) (2022) 3976–3985.
[41] A. Henniche, et al., Effect of SiC addition on mechanical properties of hot-pressed Al2O3-GdAlO3 ceramics with eutectic composition, Ceram. Int. 44 (8) (2018) 9585–9592.
[42] Y.-H. Ma, et al., Microstructural toughening mechanisms in nanostructured Al2O3/GdAlO3 eutectic composite studied using in situ microscale fracture experiments, J. Eur. Ceram. Soc. 40 (8) (2020) 3148–3157.
[43] H. Udin, A.J. Shaler, J. Wulff, The surface tension of solid copper, Trans. Am. Inst. Min. Metall. Pet. Eng. 1 (2) (1949) 186–190 (Trans).
[44] D.L. Johnson, Obtaining volume, grain-boundary, and surface diffusion coefficients from sintering data, J. Appl. Phys. 40 (1) (1969) 192–200.
[45] M.M. Opeka, I.G. Talmy, J.A. Zaykoski, Oxidation-based materials selection for 2000°C + hypersonic aerosurfaces: theoretical considerations and historical experience, J. Mater. Sci. 39 (19) (2004) 5887–5904.
[46] O. Hussein, et al., Unraveling the role of grain boundary anisotropy in sintering: implications for nanoscale manufacturing, ACS Appl. Nano Mater. 4 (8) (2021) 8039–8049.
[47] M.N. Rahaman, L.C. De Jonghe, R.J. Brook, Effect of shear stress on sintering, J. Am. Ceram. Soc. 69 (1) (1986) 53–58.
[48] D.N.F. Muche, et al., Colossal grain boundary strengthening in ultrafine nanocrystalline oxides, Mater. Lett. 186 (2017) 298–300.